Ionic Strength and Solution Composition Dictate the Adsorption of Cell-Penetrating Peptides onto Phosphatidylcholine Membranes

Man Nguyen Thi Hong,[†] Denys Biriukov,[†] Carmelo Tempra,[†] Katarina Baxova,[†] Hector Martinez-Seara,[†] Hüseyin Evci,[‡] Vandana Singh,[‡,¶] Radek Šachl,[‡] Martin Hof,[‡] Pavel Jungwirth,[†] Matti Javanainen,[*,†,§] and Mario Vazdar[*,†,‖]

†*Institute of Organic Chemistry and Biochemistry of the Czech Academy of Sciences, Flemingovo nám. 542/2, CZ-16000 Prague 6, Czech Republic*

‡*J. Heyrovský Institute of Physical Chemistry of the Czech Academy of Sciences, Dolejškova 2155/3, CZ-18223 Prague 8, Czech Republic*

¶*Faculty of Mathematics and Physics at Charles University, Prague, Czech Republic*

§*Institute of Biotechnology, University of Helsinki, FI-00014 University of Helsinki, Finland*

‖*Department of Mathematics, University of Chemistry and Technology, 166 28 Prague, Czech Republic*

E-mail: matti.javanainen@helsinki.fi; mario.vazdar@vscht.cz

Abstract

Adsorption of arginine-rich positively charged peptides onto neutral zwitterionic phosphocholine (PC) bilayers is a key step in the translocation of those potent cell-penetrating peptides into the cell interior. In the past, we have shown both theoretically and experimentally that polyarginines adsorb to the neutral PC-supported lipid bilayers in contrast to polylysines. However, the comparison of our results with previous studies showed that the results often do not match even at the qualitative level. The adsorption of arginine-rich peptides onto POPC may qualitatively depend on the actual experimental conditions where binding experiments have been performed.

In this work, we systematically studied the adsorption of R_9 and K_9 peptides onto the POPC bilayer, aided by molecular dynamics (MD) simulations and fluorescence cross-correlation spectroscopy (FCCS) experiments. Using MD simulations, we tested a series of increasing peptide concentrations, in parallel with increasing Na^+ and Ca^{2+} salt concentrations, showing that the apparent strength of adsorption of R_9 decreases upon the increase of peptide and/or salt concentration in the system. The key result from the simulations is that the salt concentrations used experimentally can alter the picture of peptide adsorption qualitatively. Using FCCS experiments with fluorescently labeled R_9 and K_9, we first demonstrated that the binding of R_9 to POPC is tighter by almost two orders of magnitude compared to that of K_9. Finally, upon the addition of excess of either Na^+ or Ca^{2+} ions with R_9, the total fluorescence correlation signal is lost which implies the unbinding of R_9 from the PC bilayer, in agreement with our predictions from MD simulations.

Graphical TOC Entry

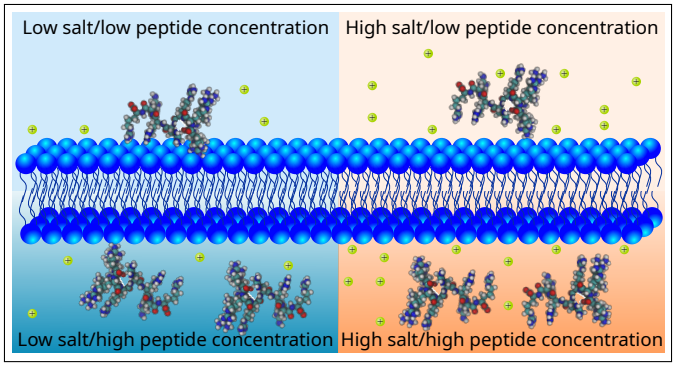

Introduction

The inefficient transfer of bioactive molecules to their therapeutic targets is one of the main challenges in cell biology.[1] In search of strategies for enhancing delivery activity, cell-penetrating peptides (CPPs) have been found to be promising agents with the ability to not only translocate across cell membranes but also to transport cargo with a variety of sizes such as small-drug molecules, nucleic acids, and proteins into the cytosol of living cells without substantially damaging the cellular membrane.[2–6] Among the CPP family, arginine-rich cell-penetrating peptides (ARCPPs) have been extensively investigated since the arginine-rich sequence of the transduction domain of the HIV-1 transactivator of transcription protein was first discovered to efficiently cross the cellular membrane.[7,8] As a special class of AR-CPPs, polyarginines of more than six residues have become well-studied as particularly active CPPs.[9–12]

Despite the significant research effort, the molecular level penetration mechanism of CPPs remains obscure.[13–16] In general, two major models have been proposed—direct penetration across lipid bilayers as an energy-independent process and endocytosis as an energy-dependent process regulated by cells.[17–19] It has been found that the uptake efficiency is strongly modulated by experimental conditions, such as temperature, concentration, type of cells, peptides, and the type of cargo.[19–22] In contrast to tightly cellular-regulated endocytosis, the energy-independent direct translocation mechanism is more interesting from the molecular point of view due to its physically unusual route, which involves the translocation of highly charged CPPs across the hydrophobic core of a lipid bilayer. As this process is energetically unfavorable, it has proven to be difficult to study using conventional computational techniques.[23,24]

A broad interest in ARCPPs has initiated numerous experimental and theoretical studies investigating not only the molecular mechanisms of the cell penetration but also the ability of ARCPPs to adsorb to cell membranes which is a crucial initial step in the translocation process regardless of the subsequent mechanism. Unfortunately, currently available exper-

imental data of peptide adsorption and peptide translocation across biological membranes have been obtained under various conditions, such as different peptide-to-lipid ratios, ionic strengths, or different vesicle sizes, and are, therefore, mutually inconsistent. For example, it has been shown by fluorescence measurements at supported lipid bilayers that R_9 adsorbs at neutral phosphatidylcholine (PC) bilayers with a micromolar dissociation constant, whereas K_9 does not adsorb at all at low peptide concentrations.[25] In contrast, in time-dependent fluorescent shift experiments performed on large unilamellar vesicles (LUVs) at high peptide concentrations of R_{10} and K_{10}, it has been shown that the differences in the interaction with PC bilayers are negligible.[26] Similarly, experimental results on the penetration of ARCPPs also differ depending on the experimental conditions. In particular, penetration of ARCPPs across LUVs composed of PC, phosphatidylethanolamine (PE), and negatively charged phosphatidylserine (PS) lipids has been explained by induction of membrane multilamellarity, negative curvature induction, and subsequent formation of a fusion pore similar to membrane fusion induced by calcium.[27] Importantly, the penetration of ARCPPs has been observed only after the addition of PE and PS lipids but not for LUVs composed solely of zwitterionic PC, which would better represent the extracellular leaflet of the plasma membrane.[27] Recently, it has been proposed that multilamellarity induction is also responsible for the endosomal escape of ARCPPs in cells and late endosome-like LUVs composed of PC and negatively charged bis(monoacylglycero)phosphate lipids.[28,29] On the other hand, Pujals et al. have shown that induction of positive curvature and lipid phase transition upon ARCPP adsorption at phospholipid bilayers are responsible for pore-free translocation.[30] In terms of simulations, different studies have predicted different tendencies for polyarginine adsorption onto zwitterionic PC membranes. Robison et al. observed the enrichment of R_9 on a POPC surface using an atomistic simulation model,[25] whereas coarse-grained simulations found no such effect.[31] Regardless of these differences, no simulation studies have observed the direct permeation of polyarginines, and the free energy barrier extracted for direct R_{10} penetration across the DOPC bilayer was estimated from

biased simulations to be a massive ≈130 kJ/mol.[31] Other simulation studies have suggested that a potential applied across the membrane could facilitate permeation,[32,33] yet it is not directly evident how a mechanism based on a potential gradient would discriminate between polyarginines and polylysines. Still, the membrane potential seems to play a role in cells, as demonstrated by a recent experimental study highlighting the role of ion channels in generating permeable pores.[21] Moreover, very recent experiments with giant unilamellar vesicles (GUVs) composed of neutral PC lipids at very low ARCPP concentrations have actually shown pore-free translocation of ARCPPs,[34,35] in contrast to previous literature.

Based on the available experimental and simulation data, it is clear that the interaction of peptides with membranes is sensitive to the experimental conditions they were measured under. Here, we try to understand these differences by systematically examining how the adsorption of cationic peptides onto POPC membranes depends on both peptide and ionic concentrations using a combination of molecular dynamics (MD) simulations and fluorescence cross-correlation spectroscopy (FCCS) experiments.[36] A major methodological issue with classical MD simulations lies in the fact that electronic polarizability is not properly described resulting in the overestimation of ion–ion interactions, leading to severe artifacts in the description of interactions between charged ions or functional groups in MD simulations.[37] In order to account for electronic polarizability, it has been proposed that scaling ionic charges by a factor of 0.75 accounts for the missing electronic polarizability in a mean-field manner.[38] This approach, denoted as "Electronic Continuum Correction" (ECC), has been shown to improve the description of adsorption of ions onto lipid bilayers, as well as the interactions among amino acids.[39–42] Indeed, the CHARMM36-based ProsECCo lipid and protein models used here rely on the scaled charges. The ProsECCo models provide a realistic structural response of lipid head groups to ion adsorption, while the osmotic coefficient measurements on amino acids also show improved agreement with the experiment as compared to the respective full-charge CHARMM36 models. With ProsECCo, there are regular adsorption and desorption events of ions and peptides to and from a POPC membrane surface so that the

system behavior can be studied by unbiased MD simulations at the microsecond time scale. This benefit renders MD simulations with ProsECCo perfectly suited for the efficient probing of different conditions in the system, particularly a wide range of peptide concentrations and ionic strengths. In concert, dual-color FCCS experiments were chosen due to their high sensitivity, low amounts of sample, and short measurement times. In contrast to fluorescent correlation experiments (FCS), they also allow for a more precise determination of binding constants since they do not rely solely on the change in diffusion coefficient but rather on the correlative motion between fluorescently labeled peptides and liposomes which eliminates the unwanted experimental problems occurring during peptide aggregation at membranes.[36] Importantly, it should be stressed that the R_9/K_9 adsorption measurements in the current experiments use liposomes instead of supported lipid bilayers used in our previous work.[25] This choice eliminates any support–lipid interactions that might cause pore formation,[43] and ensures that the model system has a similar size and thus average curvature as a cell.

Since the outer layer of cellular membranes primarily consists of neutral/zwitterionic phospholipids and sphingolipids,[44] the CPPs first need to adsorb to the surface made up of PC head groups. Thus, in this work, we employed the POPC bilayer as the simplest model for the extracellular leaflet of the plasma membrane to get more insight into the first stage of the translocation mechanism using MD simulations. As model peptides, we used nona–arginines (R_9) and nona–lysines (K_9) since this peptide length is optimal regarding translocation efficiency across lipid membranes.[45] We also use different concentrations of NaCl and $CaCl_2$, thus covering a large number of possible experimental conditions. We accompanied the simulations by FCCS experiments performed at varying peptide concentrations in different ionic solutions. Finally, MD simulations employing ECC give a realistic description of peptide binding to providing a detailed picture of the adsorption of positively charged peptides to neutral PC bilayers and also explaining the differences observed in the available experimental data.

Computational Methods

Unbiased Simulations

Atomistic molecular dynamics (MD) simulations were employed to systematically investigate the membrane interactions of nona-arginines (R_9) and nona-lysines (K_9) in aqueous solutions of either NaCl or $CaCl_2$. In order to investigate the influence of both peptide and salt concentrations on the binding, a total of 110 simulations were performed for the varying concentrations of R_9 or K_9 peptides (0.007–0.056 m *i.e.*, Arg/Lys amino acid concentration of 0.063–0.504 m) and NaCl or $CaCl_2$ salts (0–1.065 m). The details of all studied systems are summarized in Table S1 in the Supporting Information (SI). The peptides (2 to 16 molecules corresponding to the concentrations above) were initially equally distributed on both sides of the POPC bilayer and relatively close to the interface. Chloride counterions were added to neutralize the systems. The simulation boxes of all studied systems contained 15856 water molecules. The membrane bilayer consisted of 100 1-palmitoyl-2-oleoyl-sn-glycero-3-phosphocholine (POPC) lipids in each leaflet.

In this work, the CHARMM36-based ProsECCo models were applied for lipids and proteins,[41,42,46] and the ion parameters also followed the electronic continuum correction (ECC) approach.[47–49] These models aim at fixing the overbinding problem of charged molecules to zwitterionic bilayers.[39,50,51] Specifically, the partial charges in the ProsECCo models, namely those of the phosphate and choline groups of POPC and the charged groups of arginine and lysine (both the termini and the side-chains), were adjusted so that the total charge of each of these groups was scaled down from ± 1 to ± 0.75. The partial charges are provided in Table S2. No other changes were made to the CHARMM36 lipid or peptide parameters. NBFIX was disabled, as it provides an empirical correction to ion and protein overbinding, yet the ECC approach achieves a similar effect in a physically well-justified manner.[39,40] All the systems were solvated with the CHARMM-specific TIP3P ("TIPS3P") water.[52,53]

Buffered Verlet lists were used to track atomic neighbors.[54] A cut-off of 1.2 nm was used

for the Lennard-Jones potential, and the forces were switched to zero between 1.0 and 1.2 nm. The smooth particle mesh Ewald[55,56] was used for long–range electrostatics. The systems were equilibrated using the Berendsen thermostat and barostat.[57] For production runs, we used the Parrinello–Rahman barostat[58] with semi-isotropic pressure coupling and a 1 bar reference pressure, as well as the Nosé–Hoover thermostat[59,60] with a target temperature of 310 K. The time constants for coupling were set to 5 ps and 1 ps for the barostat and the thermostat, respectively. Lipid molecules, peptides, and solvent (water & ions) were coupled separately to the thermostats. All covalent bonds in peptides and lipids involving hydrogens were constrained using the P-LINCS algorithm,[61,62] whereas the SETTLE algorithm[63] was used for water molecules. MD simulations were performed for 2 μs using the GROMACS package.[64,65] The time step in all the simulations was set to 2 fs.

The production trajectories were analyzed by in-house Python scripts in conjunction with MDAnalysis library.[66] The first 500 ns of every trajectory were omitted from the analyses.

Well-Tempered Metadynamics

The well-tempered metadynamics technique[67] was employed to directly assess the adsorption free energy of polypeptides at a POPC bilayer. Six systems were modeled, each having either two nona-arginines or two nona-lysines solvated in 1.065m NaCl, 1.065m $CaCl_2$, or salt-free aqueous solution. The two collective variables were the z-components of the center-of-mass distances between the membrane and each polypeptide in the system. The selection of the collective variables, together with the system composition, enabled probing the adsorption of one or two polypeptides, which is hardly accessible from unbiased simulations due to rare or zero occurence of bound/unbound events. Each extracted two-dimensional energy profile was symmetrized along the identity line and then shifted to zero at the bulk value, *i.e.*, the free energy when both peptides are further than 4 nm from the membrane was set to zero. To enhance the sampling and convergence, the initial position of the polypeptides was chosen to be close to one of the lipid leaflets. Each collective variable was restrained by a harmonic

potential with a force constant of 50,000 and 10,000 $kJ\,mol^{-1}\,nm^{-2}$ acting at distances larger than 5.2 and 5.5 nm for salt-free and concentrated solutions, respectively. This prevented the adsorption of either peptide to another leaflet. The initial height of the Gaussians was set to 1 kJ/mol, and their width was 0.1 nm. The bias factor was equal to 10. The total length of the simulations was 1.5 µs for all systems except R_9 in salt-concentrated solutions, where the simulations were extended up to 3 µs. The Gaussians were added every 1 ps. Aside from the applied bias, the simulation protocol was otherwise identical to the protocol used for unbiased simulations. The metadynamics simulations were performed in Gromacs software with PLUMED plugin.[68]

Experimental Methods

Materials: POPC (1,2-dioleoyl-sn-glycero-3-phosphoethanolamine) lipids labeled with ATTO 488 (DOPE-ATTO 488), and 1,2-dioleoyl-sn-glycero-3-phosphoethanolamine labeled with ATTO 633 (DOPE-ATTO 633) were purchased from Avanti Polar Lipids (Alabaster, AL, USA). 4-(2-Hydroxyethyl)-piperazine-1-ethanesulfonic acid sodium salt (HEPES), sodium and calcium chloride, sucrose, and 50 nM Whatman Nuclepore Track-Etched Membranes were purchased from Sigma-Aldrich (St. Louis, MO) with a purity of 99 %. The µ-Slide 8 well ibidi chambers with Ibireat bottom were purchased from ibidi GmbH (Gräfelfing, Germany). H-$(Lys)_9$-OH (or K_9), H-$(Arg)_9$-OH (or R_9), 5(6)-carboxy-2',7'-difluorofluorescein-$(Lys)_9$-OH (or OregonGreen488-K_9), and 5(6)-carboxy-2',7'-difluorofluorescein-$(Arg)_9$-OH (or OregonGreen488-R_9) were synthesized by solid-phase peptide synthesis (SPPS) on PS3 peptide synthesizer (Gyros Protein Technologies, USA) using standard Fmoc chemistry protocols, HBTU coupling reagents and 2-chlorotrityl chloride resin support (0.1 mmol scale, 10 equivalent amino acid excess). In the case of peptides labeled with fluorescent dyes, the 5(6)-carboxy-2',7'-difluorofluorescein[69] was attached at the last coupling step. Side chain protected peptides were cleaved off the resin with a mixture of acetic acid/2,2,2-trifluoroethanol/dichloromethane (1:1:3) for 2 hrs at room temperature. The resin was

filtered off, reagents and solvents were evaporated to dryness, and residues were treated with the mixture of water/trifluoroacetic acid/triisopropylsilane (95:2.5:2:5). The cleaved and deprotected peptides were lyophilized and purified by RP HPLC (Vydac 218TP101522 column) using methanol and water with 0.05 % TFA as solvents. The purity was assessed by analytical RP-HPLC (Vydac 218TP54 column) and LC/MS (Agilent Technologies 6230 ToF LC/MS). The mass was confirmed by MALDI-ToF MS: H-(Lys)9-OH $[M+H]^+$ 1171.9; H-(Arg)9-OH $[M+H]^+$ 1423.9; OregonGreen488-K9 $[M+H]^+$ 1565.9; OregonGreen488-R9 $[M+H]^+$ 1817.9

Liposome Preparation: Large unilamellar vesicles (LUVs) were prepared by mixing POPC and DOPE-ATTO 633 at the lipid to dye ratio of 4000:1. Calculated amounts of lipids were put into a glass tube and evaporated with nitrogen. To remove any organic solvent, the samples were put under vacuum for overnight. Buffer containing 10 mM HEPES was added to form Multilamellar Vesicles (MLVs), together with the appropriate concentrations of NaCl and $CaCl_2$ when needed. MLVs were extruded through 50 nM Whatman Nuclepore Track-Etched Membranes mounted in a mini–extruder (Avestin, Ottawa, ON, Canada) fitted with two 0.5 ml Hamilton gastight syringes (Hamilton, Reno, NV). The sizes of the resulting LUVs were checked by Dynamic Light Scattering (DLS) with Zetasizer Nano ZS (Malvern Instruments Ltd.) containing a He–Ne laser (532 nm) and an avalanche photodiode detector (APD). The concentration of LUVs used in the experiments is 0.5 mM. Imaging chambers (Ibidi Uncoated) were incubated sequentially with 0.1mg/ml BSA (Sigma) dissolved in Milli-Q water to the addition of the sample.

Set-Up For Fluorescence Cross-Correlation Spectroscopy (FCCS): The microscope Olympus IX71 body consists of standard confocal parts: a 635 dichroic mirror (Chroma, USA), a water immersion objective (UPLSAPO 60×, Olympus, Japan), 3D sample scanning stage (PI Mars XYZ NanoPositioner, PI, Germany), and 50 µm pinhole. The detection unit consists of 697/58 and 525/50 nm emission filters (Chroma, USA), and a pair of Single Photon Avalanche Diodes (PDM, MPD, Italy). Samples were excited by 470 nm (LDH–

P–C–470, Picoquant, Germany) and 635 nm (LDH–D–C–635, Picoquant, Germany) lasers operated at 10 MHz repetition rate each and pulsed alternatively. The laser power was kept between 1–4 µW.

Measurements of Peptide Binding Curves Using FCCS: ATTO 488 and Alexa Fluor 647 were used to determine the effective detection volume sizes for blue and red laser, respectively. The effective cross-correlation detection volume, $V_{\mathrm{eff},x}$, was calculated from:

$$V_{\mathrm{eff},x} = \pi^{3/2} \left(\frac{\omega_{xy,\mathrm{b}}^2 + \omega_{xy,\mathrm{r}}^2}{2} \right)^{3/2} S. \tag{1}$$

In this equation, S is the structural parameter,[70] and $\omega_{xy,\mathrm{b}}$ and $\omega_{xy,\mathrm{r}}$ are the focus radii of blue and red lasers, respectively. $\omega_{xy,\mathrm{b}}$ and $\omega_{xy,\mathrm{r}}$ were determined using the tabulated values of the diffusion coefficients (D) for ATTO 488 and Alexa Fluor 647, respectively, and measured diffusion time of the dyes. Before any measurement, double-labeled LUVs (POPC with DOPE–ATTO 633 and DOPE–ATTO 488) were used to determine the maximum achievable cross-correlation amplitude characterizing the microscope alignment. The concentration of lipids was kept at 0.6 mM. Unlabeled R_9 and R_9 labeled with Oregon Green 488 were mixed at 10:1 molar ratio. Different amounts of this mixture were incubated with LUVs for 10 min before any measurement. Each point was measured for at least 1 minute.

Analysis of FCCS data:. The analysis is based on calculating a so-called cross-correlation function $G_x(\tau)$ defined as

$$G_x(\tau) = \frac{\langle F_1(t) \times F_2(t+\tau) \rangle}{\langle F_1 \rangle \langle F_2 \rangle} - 1. \tag{2}$$

This function correlates the intensity in one channel at time t ($F_1(t)$) with the intensity in the other channel at time τ later ($F_2(t+\tau)$). In this work, we correlated the intensity in the blue channel (corresponding to fluorescently labelled R_9/K_9 peptide) with the intensity in the red channel (corresponding to fluorescently labelled vesicles). In this way, we could follow

binding of R_9/K_9 peptides to lipid vesicles. Whereas a positive cross-correlation amplitude indicates binding, zero cross-correlation amplitude indicates that most of peptide molecules are left in the solution without interacting with the vesicles. FCCS may also be used to calculate the dissociation constant of binding. This analysis is based on the determination of the actual number of bound peptides per LUV, $\langle \mathrm{NP} \rangle$, and the concentration of free peptide in the solution, C_P^{free} from FCCS data. In case of non-cooperative binding, C_P^{free} and $\langle \mathrm{NP} \rangle$ are related through a Langmuir isotherm. This reads

$$\langle \mathrm{NP} \rangle = N_{\mathrm{max}} \frac{C_P^{\mathrm{free}}/N_{\mathrm{A}}}{K_D + C_P^{\mathrm{free}}/N_{\mathrm{A}}}, \tag{3}$$

where K_D is the dissociation constant, N_{max} is the maximum number of binding sites per LUV, and N_{A} is the Avogadro's number. Thus, K_D and N_{max} can be determined by fitting experimental FCCS data to Eq. (3). $\langle \mathrm{NP} \rangle$ can be determined from the known cross-correlation amplitude (G_x^0 , $\mathrm{V_{eff,}}_x$) and the total peptide concentration C_P^0 as in Ref. 36:

$$\langle \mathrm{NP} \rangle = G_x^0 V_{\mathrm{eff,x}} C_P^0. \tag{4}$$

Similarly, C_p^{free} is calculated as in Ref. 36

$$C_P^{\mathrm{free}} = C_P^0 \left(1 - \frac{1 + \langle N_r \rangle G_x^0 V_{\mathrm{eff},x}}{\langle N_r \rangle G_r^0 V_{\mathrm{eff},r}} \right), \tag{5}$$

where $\langle N_r \rangle$ is the number of lipid dye molecule per LUV, while G_r^0 is the red auto-correlation amplitude determined using Origin software, and $V_{\mathrm{eff},r}$ is the effective detection volume of the red laser.

Results and Discussion

Polyarginine and Polylysine Display Qualitatively Different Adsorption Tendencies

We performed an extensive set of atomistic simulations of a POPC bilayer with varying numbers of R_9 and K_9 peptides either in pure water or in solutions containing NaCl or $CaCl_2$. The free energies of adsorption of R_9 and K_9 peptides onto a POPC bilayer were computed from symmetrized averaged number density profiles of peptides along the z direction from the bulk solution to the membrane surface using the expression:

$$\Delta G = -k_{\mathrm{B}}T \ln(P_{\mathrm{bound}}/P_{\mathrm{unbound}}). \tag{6}$$

Here, k_{B} is Boltzmann constant, T is absolute temperature, P_{bound} and P_{unbound} were defined as probabilities of the peptide being in bound and unbound regions with respect to the membrane surface, respectively. These probabilities are obtained by integrating the normalized peptide number density distribution ρ over the relevant region, namely:

$$P_{\mathrm{bound}} = \int_0^{z(\rho_{\mathrm{min}})} \rho \mathrm{d}z \quad \text{and} \quad P_{\mathrm{unbound}} = \int_{z(\rho_{\mathrm{min}})}^{z_{\mathrm{max}}} \rho \mathrm{d}z, \tag{7}$$

where the cut-off distance $z(\rho_{\mathrm{min}})$ is the z minimum coordinate of the density distribution function ρ, $z = 0$ refers to the membrane center, and z_{max} is the maximum value of the z coordinate in the simulation box. For density profiles with no specific binding peaks (usually the case for K_9), the cut-off value was chosen as 3.5 nm which is the average calculated over the other $z(\rho_{\mathrm{min}})$ values.

Free energy differences, ΔG, calculated from all of our 55 simulations for R_9 and K_9 are presented in Fig. 1 as heatmaps of two variables, *i.e.*, the nominal peptide and salt concentrations. Looking first at the systems without salt (top rows in the panels in Fig. 1),

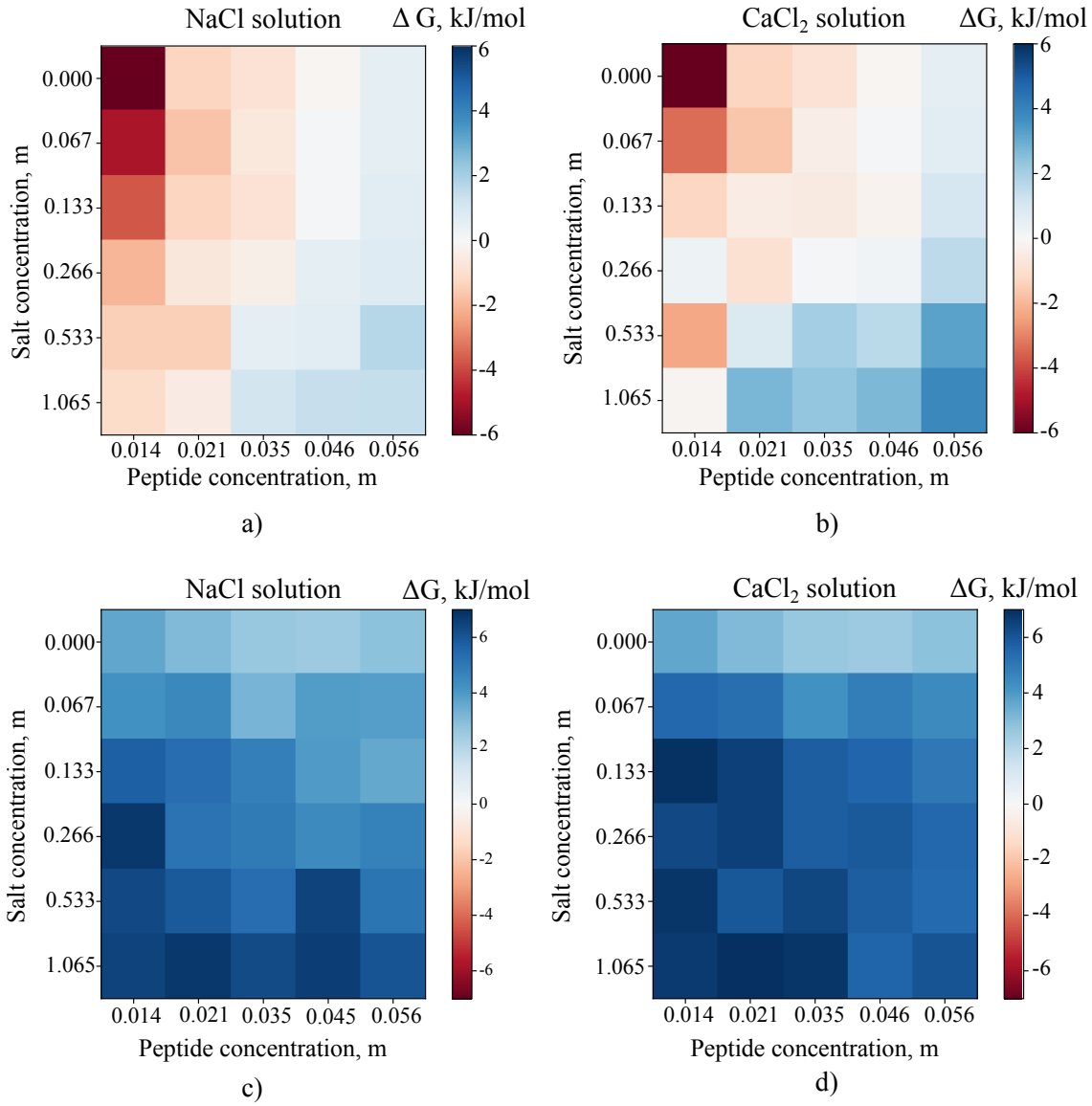

Figure 1: The free energy ΔG (kJ mol^{-1}) of the binding of R_9 (top row) or K_9 (bottom row) peptides to the POPC membrane surface with various concentrations of the peptide and ions in the solution.

it is evident that R_9 preferentially binds to POPC at peptide concentrations up to 0.035 m ($\Delta G < 0$). At the lowest R_9 concentration, *i.e.*, with four peptides present in the system, the binding is the most stable at -6 kJ/mol, whereas the value rapidly decreases upon increasing R_9 concentration. Notably, the ΔG value changes sign at 0.046 m, indicating that at higher

peptide concentrations, the R_9s prefer to remain in the solution rather than adsorb onto the membrane. This behavior is also demonstrated by the top row in Fig. S1 which shows the effect of peptide concentration on their density profiles. At higher peptide concentrations, many of the peptides reside in the solution for most of the simulation time. This observation can be explained by two factors: peptide adsorption saturation at the membrane surface and an increase in ionic strength in the bulk due to presence of positively charged peptides. Such a behavior is expected and provides the typical Langmuir-like isotherm at low salt concentrations. Still, the free energy values reported here for different peptide concentrations are useful in describing the peptide populations in the solution and on the POPC surface, with implications for the interpretation of experimental data.

Comparing next the behavior of R_9 (top two panels in Fig. 1) with that of K_9 (botom two panels in Fig. 1), it is evident that the two peptides display opposite binding behavior. Indeed, it is clear that K_9 peptides do not adsorb onto the POPC surface at any peptide concentration, with positive values of ΔG ranging from 2.9 to 7.5 kJ/mol. These low binding affinities of K_9 are also demonstrated by the density profiles (see Fig. S4) where density at binding sites (lipid head group position) is depleted compared to the bulk phase. Several experimental and theoretical investigations have reported similar findings.[25,71,72]

Moreover, the peptide concentration appears to have an opposite effect on the membrane-binding of K_9 than what was observed for R_9. In other words, the increasing of amount of K_9 peptides causes a decrease of ΔG values. However, this trend follows from the simple fact that inter-peptide repulsion at higher concentration slightly pushes peptides to the vicinity of the membrane surface, thus leading to an increased density in that region even without specific binding. This is corroborated by the density profiles shown in Fig. S4.

While our unbiased simulations are performed using state-of-the-art computer resources, the sampling of the binding equilibrium is challenging with only a few peptides, *i.e.*, when the binding is most favorable. Fortunately, in this low-concentration regime, the system behavior can be described by a couple of intuitive reaction coordinates and thus probed using biased

simulation approaches. We chose to perform well-tempered metadynamics simulations to probe the binding of two R_9 or K_9 peptides to the same POPC leaflet. As demonstrated in Fig. S3, the metadynamics simulations indeed converge well within the simulation time. The free energy surfaces extracted from these simulations in the absence of salt are shown in the leftmost panel of Fig. 2, and confirm that for R_9 there is a clear global free energy minimum of ~ -30 kJ/mol at the membrane surface, at around 2.2 nm away from the membrane core. In constrast, no such minimum is observed for K_9. Instead, the most favorable positioning for K_9 is in the aqueous phase, as far from the POPC surface as allowed by our simulation setup.

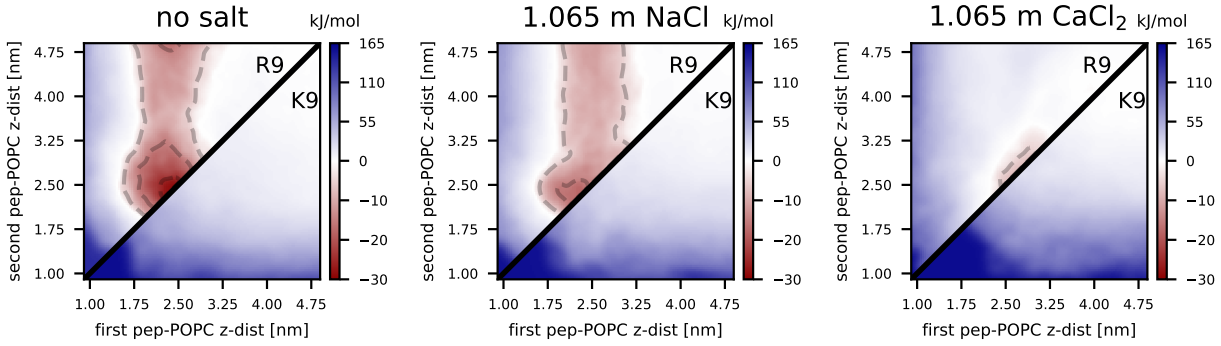

Figure 2: The resulting post-processed two-dimensional free energy profiles for R_9 or K_9 peptides adsorbed to the POPC membrane under different ionic concentration conditions. The contours are added for –5, –15, and –25 kJ/mol. The evolution of the total adsorption free energy—demonstrating convergence—is shown in Fig. S3.

Having convincingly demonstrated the difference between R_9 and K_9 adsorption onto the zwitterionic membranes using our implicitly polarized simulation model, we verified these findings experimentally. To this end, we performed fluorescence cross-correlation spectroscopy (FCCS) measurements for systems where POPC vesicles were exposed to either R_9 or K_9, without the presence of salt ions. In these experiments, 10% of R_9 and K_9 are labeled with Oregon Green 488 fluorescent label, with the zwitterionic POPC membrane containing fluorescently labeled lipids (see Experimental details).

Figure 3 shows the experimentally determined Langmuir binding isotherms for labeled R_9 and K_9. The Langmuir fit assumes independent binding sites and no interactions among

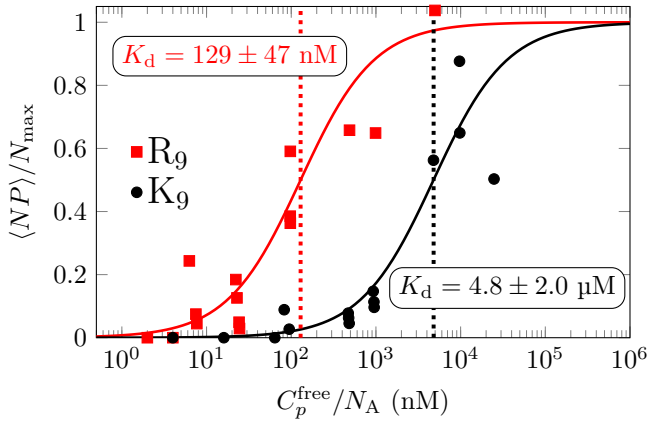

Figure 3: Experimentally determined Langmuir binding isotherms for R_9 (red squares) and K_9 (black circles) peptides and the corresponding fits (solid lines; assuming independent sites and non-cooperative binding) relating the number of binding sites for the peptide per LUV and the concentration of free peptide in the bulk. The data are normalized so that Eq. (3) converges to 1 at large concentrations.

the peptides (i.e. non-cooperative binding). The inspection of the data and the analysis of the corresponding fits show that R_9 binds almost two orders of magnitude stronger to POPC with K_d of 129 ± 47 nM in contrast to K_9, which adsorbs weaker with K_d of only 4.8 ± 2.0 µM. The adsorption of R_9 is tighter than the previously determined K_d using fluorescence binding assays of unlabeled peptides where this value was determined to be 70 ± 19 µM.[25] In addition to slightly different experimental setup (see below for details), this could be a consequence of the fact that adsorption to the surface of supported lipid bilayers[25] is, in general, mechanistically slightly different than adsorption onto free-standing LUVs used in this work. In line with this, we actually detected the adsorption of labeled K_9 in FCCS experiments in contrast to present MD simulations and fluorescence binding assays performed using supported lipid bilayers and unlabeled peptides.

To clarify the possible role of the attached Oregon Green 488 label itself in the peptide-binding strength, we performed control binding FCCS experiments with free Oregon Green 488 fluorophore in the presence of POPC vesicles. Here, as shown in Fig. 4, no positive cross-correlation was detected. However, it cannot be completely excluded that K_9 attached to the Oregon Green 488 probe increases the possibility of labeled K_9 binding to POPC.[73]

In addition, we should also mention here that the experiments in Ref. 25 and the ones performed in this work are also not fully comparable with each other. Specifically, we used a 10 mM HEPES buffer in contrast to work presented in Ref. 25 where 10 mM phosphate-buffered saline (PBS) and 150 mM NaCl was employed in the experiments. The use of different buffers in the reported experiments can also affect the adsorption of ions/peptides at membranes, especially when the buffer concentrations are comparable (or even higher, as in our case) to the peptide concentrations used in binding experiments. Indeed, some commonly used buffers can even alter the physical properties of the bilayers.[74–76] A detailed analysis of cross-correlation functions upon addition of salts and increase of ionic strength is presented in the next section.

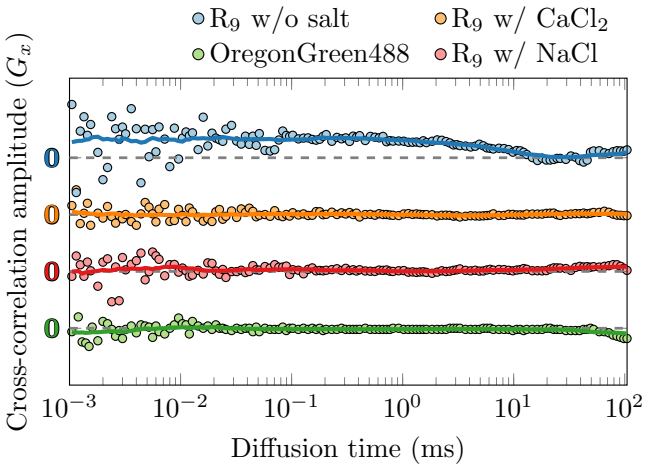

Figure 4: Calculated cross-correlation functions shown for R_9 peptides (500 nM concentration) in the absence or presence of 100 mM concentration of NaCl or $CaCl_2$. Also, a cross-correlation function for free Oregon Green 488 dye is shown. The curves are vertically shifted for clarity. The markers show measured data points, whereas the lines show running averages over 20 data points. The concentration of Oregon green 488 in all correlations is 50 nM. A positive cross-correlation indicates binding to the membrane, whereas zero cross-correlation points to non-detectable binding.

Taking into account all possible experimental differences between the different experimental setups, the most important difference in binding of R_9 vs. K_9 onto POPC is still that R_9 binds much tighter than K_9, which is in full agreement with the results reported in Ref. 25. Our data definitely confirm the binding of arginine-rich peptides to zwitterionic

POPC bilayers, which may serve as a key point in explaining why arginine-rich peptides easily penetrate POPC vesicles as well as cellular membranes, whereas lysine-rich peptides do not.

The Ionic Strength of the Solution Qualitatively Alters the Binding Behavior

Having established that R_9 and K_9 show very different binding affinities to POPC membranes and that this binding heavily depends on the peptide concentration, we moved on to the effect of salts. As seen by comparing the individual rows in Figs. 1a & 1b, the presence of salts significantly affects the adsorption of R_9 molecules onto a POPC membrane. Particularly, for a given R_9 concentration, increasing salt concentration increases the ΔG values, thus the more salt is present in the system, the weaker the membrane–peptide interaction becomes. Salt even alters the qualitative binding behavior. For example, at a peptide concentration of 0.035 m and low salt concentrations, peptide binding is favorable ($\Delta G < 0$), but at higher salt concentrations, ΔG becomes increasingly positive, suggesting that the peptides rather remain in the solution. Density profiles for individual peptides with different salt solutions are presented in Figs. S1 & S4. These profiles reveal that the decrease of the apparent averaged free energy of R_9 adsorption is not due to a decrease of individual peptide adsorption free energies. In contrast, the decrease results from the combined effect where several peptides remain strongly bound at POPC, while the rest of the peptides remain in the bulk and cannot adsorb anymore to the saturated POPC surface. The same effect of ionic strength is observed for K_9, Figs. 1c & 1d, *i.e.*, ΔG increases with increasing salt concentration.

The R_9–membrane interactions not only depend on salt concentration but also on the nature of the salt. The ΔG values for R_9–POPC systems embedded in $CaCl_2$ solutions are higher than those in NaCl solutions at the same concentrations. However, as Ca^{2+} is a divalent ion, the comparison of salt concentrations is somewhat misleading. By comparing

the peptide binding in NaCl and $CaCl_2$ solutions having the same charge concentration (compare each row in Fig. 1a with a row one step higher in Fig. 1b), our results still show that the ΔG values are higher in the $CaCl_2$ solution than in the NaCl solution. This implies that Ca^{2+} ions more efficiently decrease the binding affinity of R_9 to a POPC bilayer than Na^+ ions. A similar decrease in binding affinity was observed in an experimental study of R_8–DOPC (or DOPC/DOPG) GUVs interactions with Na^+.[77] The stronger effect of $CaCl_2$ compared to NaCl could result from two factors. First, the screening of electrostatic interactions is given by ionic strength, which scales as z^2 for an ion with a charge of z. Thus, at the same charge density, $CaCl_2$ provides a stronger screening effect than NaCl, thus reducing more efficiently the attraction between the POPC head groups and R_9. Secondly, sodium and calcium ions may also adsorb onto the head group region of zwitterionic POPC membranes and thereby introduce a positively charged surface that will repel the cationic arginine residues, in turn reducing the binding affinity of R_9. The magnitude of this effect is dictated by the total surface charge, which depends on the ion charge and adsorption preferences.

Our findings are somewhat different from those observed in atomistic simulations using the Slipids lipid model in combination with the Amber ff99SB protein model.[25] Authors of this study proposed the preferential binding of R_9 onto POPC surfaces even at peptide concentrations of ≈0.028 m or ≈0.056 m in the presence of 0.150 m of NaCl. Moreover, the effect of an increased peptide concentration was minor. A logical explanation for this discrepancy is the different force field used. Since few quantitative experimental data on the adsorption of cationic peptides are available, it is difficult to judge which model is more accurate. However, the Slipids force field is known to exaggerate the adsorption of positive ions onto PC membranes,[51] thus the stronger adsorption of cationic R_9 in the Slipids model is not surprising. ProsECCo model, in turn, is designed to resolve this somewhat unrealistic electrostatic binding.

This brings us to the question whether our ProsECCo model based on scaled charges may

predict too little R_9 adsorption onto PC membranes. To ensure that this is not the case, we performed a pair of simulations with a POPC membrane and two R_9 peptides with both CHARMM36 and ProsECCo models. As shown in Fig. S2 in the SI, the binding affinity for these models is fairly similar. However, peptides penetrate deeper into the membrane in the case of CHARMM36, with the density peaking at ca. 2 nm from the center of mass of the bilayer. With ProsECCo, the density reaches a maximum at ca. 2.3 nm, and the distributions are slightly broader, indicating a less specific binding mode. The more specific interactions in the full-charge CHARMM36 model are visible in the radial distribution functions between the arginine side chain (namely, guanidinium carbon atom) and POPC choline nitrogen atom or POPC phosphate atom, respectively (see the bottom panel in Fig. S2). This suggests that while improving the description of ion–lipid interactions, ProsECCo does not lead to qualitative differences in lipid–peptide interactions.

For additional validation, we repeated our metadynamics simulations with 1.065 m of either NaCl or $CaCl_2$. As demonstrated in the middle and rightmost panels of Fig. 2, the K_9 peptides do not prefer to adsorb to POPC membrane under any conditions, whereas the adsorption of R_9 is regulated by the ionic concentration. Our metadynamics simulations cover the extreme cases of the unbiased simulations, *i.e.* the highest salt concentration and the case of no salt. The free energy landscapes clearly show how the adsorption free energy increases from ~ -30 kJ/mol (no salt) to ~ -15 kJ/mol and ~ -10 kJ/mol in 1.065 m NaCl and 1.065 m $CaCl_2$ solutions, respectively. Interestingly, in the case of R_9 in $CaCl_2$ solution, the binding mode when only one peptide is adsorbed is not energetically favorable compared to when both peptides are adsorbed, which indicates that the dual R_9 adsorption at POPC is possibly facilitated by R_9–R_9 interactions in solution[78] or at the POPC bilayer.[25]

We also performed FCCS experiments to confirm the effect of salts to R_9 adsorption onto a POPC membrane. Figure 4 shows the cross-correlation functions for labeled R_9 at POPC in the absence and after addition of Na^+ or Ca^{2+} ions by adding 100 mM NaCl or $CaCl_2$, respectively, to 500 nM of R_9 in 10 mM HEPES solution. Two important points can be

deduced from the experiments. First, we see that cross-correlation is detected for labeled R_9 in interaction with POPC (blue curve), showing that these labeled peptides indeed adsorb to the zwitterionic PC membranes. Secondly and more importantly, we clearly see that the addition of Na^+ or Ca^{2+} induces a complete loss of the cross-correlation (orange and red curves), implying that both Na^+ and Ca^{2+} ions effectively prevent the adsorption of R_9 onto the POPC membranes under given experimental conditions. This is in accordance with our MD simulation results which show a relative decrease of total R_9 adsorption to POPC upon the increase in ionic strength either by the addition of peptides or the addition of NaCl or $CaCl_2$. This further confirms that the adsorption of peptides onto the membranes is strongly altered or can even be inhibited by the addition of salts or by a further increase in peptide concentration in the experiments.

Salt Affects Peptide Binding More Than Peptides Affect Cation Binding

Next, we analyzed in detail the effects of salt on R_9 binding and *vice versa*. The number of adsorbed R_9 molecules on the POPC surface for each system was calculated from the corresponding average number density profiles, and the results are displayed in Figs. 5a & b. In both NaCl and $CaCl_2$ aqueous environments, the number of adsorbed R_9 molecules decreases with increasing the salt concentration, as we noted previously. However, the degree of adsorption is different between Na^+ and Ca^{2+} solutions as deduced from the free energy calculations. At the same concentration, Ca^{2+} significantly reduces the adsorption of R_9 peptides, and the membrane surface is saturated at a peptide concentration of 0.046 m. Moreover, in the case of the highest salt concentration and peptide concentration of 0.056 m, the actual number of membrane adsorbed R_9 peptide starts to decrease (although still within the error estimate). While Na^+ only mildly decreases the number of adsorbed R_9 molecules, the saturation coverage may be reached at a concentration beyond the range studied in this work (0.007–0.056 m). Unlike the strong effect that cation–lipid interaction has on

peptide adsorption, the peptide–lipid binding at the interface negligibly impacts Na^+ or Ca^{2+} adsorption. Apparently, only a slight decrease in the number of bound Na^+ or Ca^{2+} is seen as the peptide concentration increases (Figs. 5c & d). This tendency is partially in line with Ref. 79, where the adsorption of sodium ions was reported as being independent of the presence of polycations.

Since numerous studies highlighted the important role of positively charged guanidinium moieties (Gdm^+) in R_9–phospholipid interactions,[12,25,26] it is interesting to check the effect of ionic strength on these interactions. Gdm^+, together with Na^+ or Ca^{2+}, preferentially interacts with the phosphate and choline groups of POPC (see Fig. S1), which leads to the competition for the adsorption sites on the POPC bilayer between R_9 and monoatomic cations. In this context, we calculated how many Gdm^+ moieties are directly bound to the surface when the peptide is bound to the POPC surface. The results are displayed in Table 1. Each adsorbed R_9 molecule, donates on average 2.5–5.9 arginine side chains to bind to the bilayer. Bound R_9s in NaCl solutions are stabilized by more Gdm^+ groups than in $CaCl_2$ solutions, and these values tend to decrease with the addition of NaCl or $CaCl_2$. This points to the fact that the binding of initially strongly bound peptides (before saturation of POPC bilayer) also tends to slightly decrease as the ionic strength increases in the bulk. Interestingly, we also observe the same trend as more peptides are added into the solutions, due to increased ionic strength by adding positively charged peptides. Taken all together, an increase in the concentration of either salts or peptides generally lowers the ability of the peptides to adsorb onto the POPC bilayer, both by diminishing electrostatic interactions of strongly bound peptides and saturating the bilayer surface.

Structural Changes of the Membrane Upon Peptide Adsorption

Finally, we address the influence of peptide and ion adsorption on the area per lipid (APL) of the POPC bilayer. In the case of ions and cationic peptides that do not penetrate to the acyl chain regions, APL is alone sufficient to describe membrane structure, as it is inversely

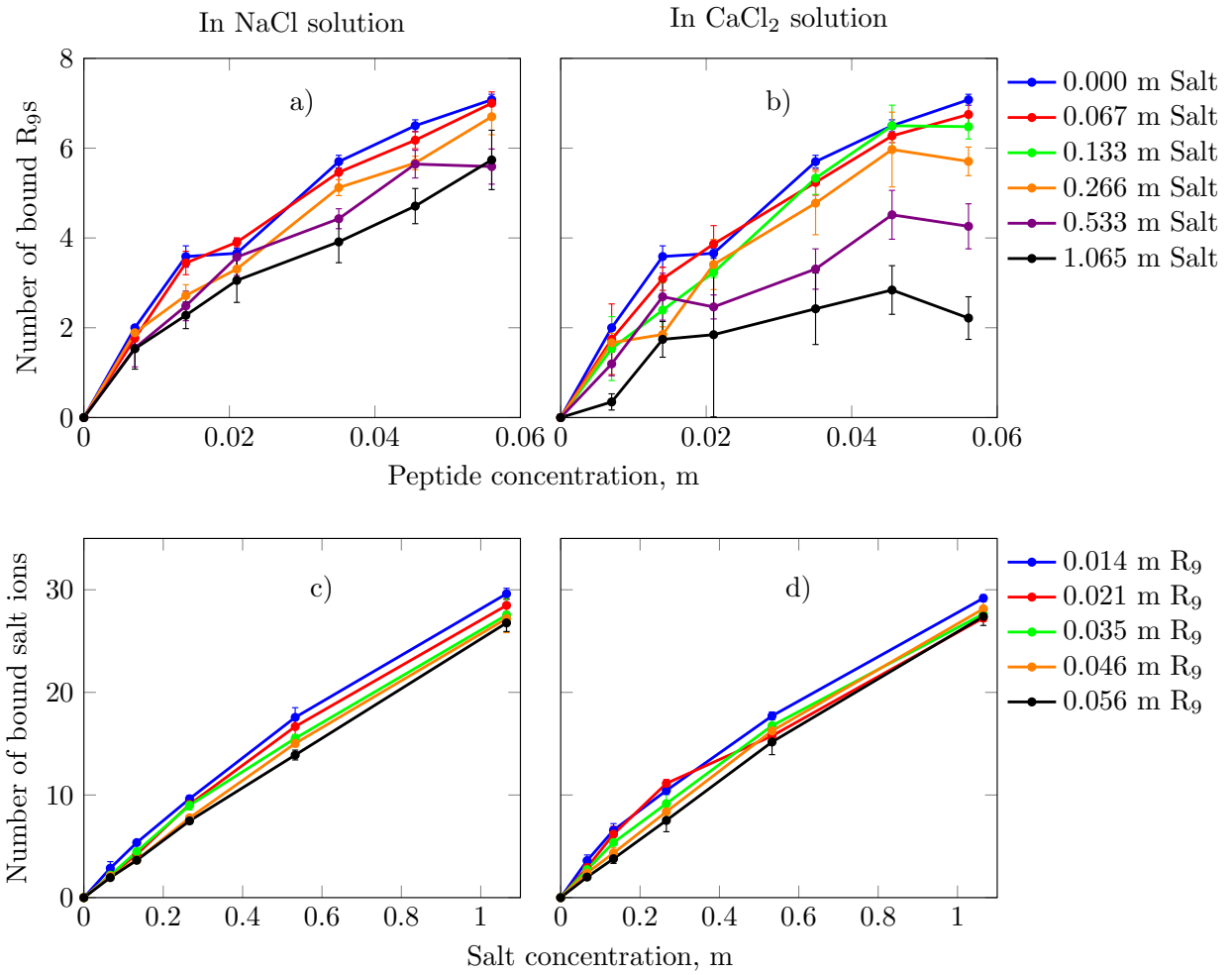

Figure 5: The change in a number of bound R_9 peptides and salt cations (Na^+, Ca^{2+}) to the membrane surface with respect to their concentrations in solution.

correlated with membrane thickness and order. The results, shown in Fig. 6, demonstrate that both adsorption processes cause changes in APL, but these effects are opposite to each other. In particular, the increase in the number of adsorbed salt ions at the surface significantly reduces APL (Ca^{2+} with its stronger binding affinity leading to a larger APL reduction than Na^+), which results from the cations fitting between the POPC head groups and bridging them together.[80] Thus, it seems that cations have a two-fold effect on the efficiency of R_9 penetration: they reduce the amount of adsorbed peptides and render the membrane more packed and hence more rigid against the formation of pores, bifurcations, or other membrane defects. In contrast, APL tends to slightly increase as the number of R_9

Table 1: The number of guanidinium groups per bound R_9 buried into the POPC membrane in the system with given peptide and salt concentrations. The values to the left correspond to NaCl solutions, the values to the right are shown for $CaCl_2$ solutions.

Concentration [m]						
Salt	R_9 peptide					
	0.007	0.014	0.021	0.035	0.046	0.056
0.000	5.9	5.3	5.3	4.9	4.4	4.3
0.067	5.5/5.5	5.3/5.2	5.4/5.1	5.0/4.5	4.7/4.3	4.5/4.3
0.133	5.9/5.9	5.6/4.3	5.2/4.8	4.8/4.7	4.7/4.2	4.2/4.1
0.266	5.8/4.9	5.4/4.6	4.5/4.8	4.5/4.5	4.6/4.4	4.2/4.0
0.533	5.2/4.3	4.9/4.7	4.8/3.5	4.1/3.5	4.4/3.8	3.7/3.3
1.065	5.0/3.0	4.8/3.8	4.4/3.4	3.6/3.0	3.9/3.1	3.7/2.5

molecules adsorbed at the POPC surface increases. This is likely caused by the penetration of R_9 into the lipid head group region followed by the expansion of the membrane due to steric stress imposed by the relatively large R_9 molecules.

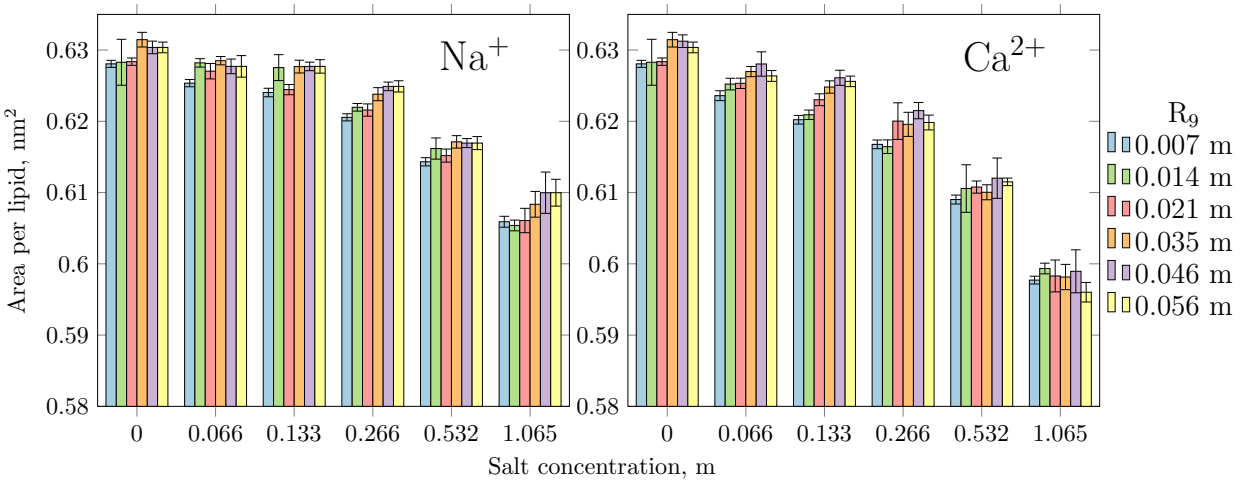

Figure 6: Changes in area per lipid with varying R_9 and salt (NaCl or $CaCl_2$) concentrations.

Conclusions

Unbiased molecular dynamics (MD) simulations, metadynamics simulations, and complementary fluorescence cross-correlation spectroscopy (FCCS) experiments were employed to

characterize the interactions of positively charged peptides—polyarginines and polylysines—with zwitterionic POPC membrane at varying concentrations of NaCl or $CaCl_2$. MD simulations reveal several important aspects of the peptide–membrane interactions. Firstly, we show by MD simulations that R_9 peptides have a stronger preference for POPC bilayer compared to K_9 peptides, which do not adsorb to POPC in any of the studied conditions. This finding agrees with earlier simulations and experiments at supported lipid bilayers[25] and also serves as an important benchmark for the employed ProsECCo interaction model incorporating polarization by scaled charges.

Secondly, the apparent peptide adsorption decreases with increasing peptide and salt concentrations. In particular, the average adsorption energy of R_9 peptides increases from ca. -6 kJ/mol in the case of no added salt and low peptide concentration to $+2$ kJ/mol in the case of high peptide concentration and the addition of 1 m NaCl, or $+6$ kJ/mol upon the addition of 1 m $CaCl_2$, respectively. In the case of K_9, the peptides do not adsorb onto POPC under any conditions. These results are confirmed by metadynamics simulations, which also demonstrated that the addition of $CaCl_2$ results in a larger increase of adsorption free energy than the addition of NaCl. The diminution of peptide adsorption is mostly due to the saturation of the POPC surface and the simultaneous increase of the peptide concentration in the bulk solution. However, the individual R_9 peptide binding affinity also slightly decreases in solutions of high ionic strength.

Our MD results are in good agreement with complementary FCCS experiments. Specifically, we observe that fluorescently labeled R_9 binds by almost two orders of magnitude tighter than K_9 to the zwitterionic POPC bilayer with $K_\mathrm{d}(R_9) = 129 \pm 47$ nmol/dm^3 and $K_\mathrm{d}(K_9) = 4.8 \pm 2.0$ µmol/dm^3, respectively. The addition of NaCl or $CaCl_2$ completely suppresses the fluorescence cross-correlation signal, indicating that the addition of either salt leads to a decrease in peptide binding on average.

Taken together, our simulations and experiments show that the increase of peptide and/or salt concentration, *i.e.*, increase of ionic strength in the system, results in diminishing bind-

ing of positively charged peptides at zwitterionic POPC bilayer dominantly due to electrostatic screening induced by additional charge in the bulk. This has important consequences and calls for careful planning of the experiments and simulations involving the binding of polycationic peptides to lipid bilayers. The experimental results can greatly depend on the initial conditions and possibly even lead to qualitatively different outcomes in terms of peptide–membrane adsorption. As the cell penetration of polyarginines (and other charged cell-penetrating peptides) involves peptides binding to the membrane as an initial step of the cell translocation mechanism, it is crucial to consider the effects of salt and peptide concentrations in the cell penetration studies as well.

Notes

The authors declare no competing financial interest.

Acknowledgement

We thank CSC–IT Center of Science for computing time. We acknowledge the support from the Czech Science Foundation (EXPRO Grant 19-26854X). MNTH acknowledges the Faculty of Mathematics and Physics of the Charles University (Prague, Czech Republic) where she is enrolled as a PhD student and the International Max Planck Research School for "Many-Particle Systems in Structured Environments" (Dresden, Germany) for support. MJ acknowledges the Academy of Finland (Postdoctoral researcher grant no. 338160) and the Emil Aaltonen Foundation for funding. MV acknowledges the Sabbatical Program at IOCB.

Supporting Information Available

SI consists of table summarizing the components of simulation boxes, additional descriptions of binding of R_9 and K_9 to POPC bilayer in terms of density profiles, metadynamics, radial distribtution functions, and minimum distance calculations. This material is available free of charge via the Internet at ACS Publications website.

References

(1) Vargason, A. M.; Anselmo, A. C.; Mitragotri, S. The evolution of commercial drug delivery technologies. *Nature Biomedical Engineering* **2021**, *100*, 1972–1977.

(2) Abes, R.; Arzumanov, A.; Moulton, H.; Abes, S.; Ivanova, G.; Iversen, P.; Gait, M.; Lebleu, B. Cell-penetrating-peptide-based delivery of oligonucleotides: an overview. *Biochemical Society Transactions* **2007**, *35*, 775–779.

(3) Torchilin, V. P.; Nielsen, H. M. Cell transfection in vitro and in vivo with nontoxic TAT peptide-liposome–DNA complexes. *Proceedings of the National Academy of Sciences* **2003**, *100*, 1972–1977.

(4) Foged, C.; Nielsen, H. M. Cell-penetrating peptides for drug delivery across membrane barriers. *Expert Opin Drug Deliv.* **2008**, *5*, 105–117.

(5) Kanekura, K.; Harada, Y.; Fujimoto, M.; Yagi, T.; Hayamizu, Y.; Nagaoka, K.; Kuroda, M. Characterization of membrane penetration and cytotoxicity of C9orf72-encoding arginine-rich dipeptides. *Sci Rep* **2018**, *8*, 12740.

(6) Langel, U. *LaTeX: Cell-penetrating peptides, processes and applications*; CRC Press Pharmacology & Toxicology Series, CRC Press: New York, 2002.

(7) Frankel, A. D.; Pabo, C. O. Cellular uptake of the tat protein from human immunodeficiency virus. *Cell* **1988**, *55*, 1189–1193.

(8) Green, M.; Loewenstein, P. M. Autonomous functional domains of chemically synthesized human immunodeficiency virus tat trans-activator protein. *Cell* **1988**, *55*, 1179–1188.

(9) Crosio, M.; Via, M.; Cámara, C.; Mangiarotti, A.; Del Pópolo, M.; Wilke, N. Interaction of a Polyarginine Peptide with Membranes of Different Mechanical Properties. *Biomolecules* **2019**, *9*, 625.

(10) Li, Z.-l.; Ding, H.-m.; Ma, Y.-q. Translocation of polyarginines and conjugated nanoparticles across asymmetric membranes. *Soft Matter* **2013**, *9*, 1281–1286.

(11) Hu, J.; Lou, Y.; Wu, F. Improved Intracellular Delivery of Polyarginine Peptides with Cargoes. *The Journal of Physical Chemistry B* **2019**, *123*, 2636–2644, PMID: 30830784.

(12) Vazdar, M.; Heyda, J.; Mason, P. E.; Tesei, G.; Allolio, C.; Lund, M.; Jungwirth, P. Arginine "Magic": Guanidinium Like-Charge Ion Pairing from Aqueous Salts to Cell Penetrating Peptides. *Accounts of Chemical Research* **2018**, *51*, 1455–1464, PMID: 29799185.

(13) Schmidt, N.; Mishra, A.; Lai, G. H.; Wong, G. C. Arginine-rich cell-penetrating peptides. *FEBS letters* **2010**, *584*, 1806–1813.

(14) Bechara, C.; Sagan, S. Cell-penetrating peptides: 20 years later, where do we stand? *FEBS letters* **2013**, *587*, 1693–1702.

(15) Stewart, K. M.; Horton, K. L.; Kelley, S. O. Cell-penetrating peptides as delivery vehicles for biology and medicine. *Organic & biomolecular chemistry* **2008**, *6*, 2242–2255.

(16) Koren, E.; Torchilin, V. P. Cell-penetrating peptides: breaking through to the other side. *Trends in molecular medicine* **2012**, *18*, 385–393.

(17) Burlina, F.; Sagan, S.; Bolbach, G.; Chassaing, G. Quantification of the Cellular Uptake of Cell-Penetrating Peptides by MALDI-TOF Mass Spectrometry. *Angewandte Chemie International Edition 44*, 4244–4247.

(18) Jiao, C.-Y.; Delaroche, D.; Burlina, F.; Alves, I. D.; Chassaing, G.; Sagan, S. Translocation and Endocytosis for Cell-penetrating Peptide Internalization. *Journal of Biological Chemistry* **2009**, *284*, 33957–33965.

(19) Ruseska, I.; Zimmer, A. Internalization mechanisms of cell-penetrating peptides. *Beilstein Journal of Nanotechnology* **2020**, *11*, 101–123.

(20) Tünnemann, G.; Ter-Avetisyan, G.; Martin, R. M.; Stöckl, M.; Herrmann, A.; Cardoso, M. C. Live-cell analysis of cell penetration ability and toxicity of oligo-arginines. *Journal of Peptide Science* **2008**, *14*, 469–476.

(21) Trofimenko, E.; Grasso, G.; Heulot, M.; Chevalier, N.; Deriu, M. A.; Dubuis, G.; Arribat, Y.; Serulla, M.; Michel, S.; Vantomme, G. et al. Genetic, cellular and structural characterization of the membrane potential-dependent cell-penetrating peptide translocation pore. *bioRxiv* **2021**,

(22) Wallbrecher, R.; Ackels, T.; Olea, R. A.; Klein, M. J.; Caillon, L.; Schiller, J.; Bovée-Geurts, P. H.; van Kuppevelt, T. H.; Ulrich, A. S.; Spehr, M. et al. Membrane permeation of arginine-rich cell-penetrating peptides independent of transmembrane potential as a function of lipid composition and membrane fluidity. *Journal of Controlled Release* **2017**, *256*, 68–78.

(23) Pokhrel, N.; Maibaum, L. Free Energy Calculations of Membrane Permeation: Challenges Due to Strong Headgroup–Solute Interactions. *Journal of Chemical Theory and Computation* **2018**, *14*, 1762–1771, PMID: 29406707.

(24) Lee, C. T.; Comer, J.; Herndon, C.; Leung, N.; Pavlova, A.; Swift, R. V.; Tung, C.; Rowley, C. N.; Amaro, R. E.; Chipot, C. et al. Simulation-Based Approaches for Determining Membrane Permeability of Small Compounds. *Journal of Chemical Information and Modeling* **2016**, *56*, 721–733, PMID: 27043429.

(25) Robison, A. D.; Sun, S.; Poyton, M. F.; Johnson, G. A.; Pellois, J.-P.; Jungwirth, P.; Vazdar, M.; Cremer, P. S. Polyarginine Interacts More Strongly and Cooperatively than Polylysine with Phospholipid Bilayers. *The Journal of Physical Chemistry B* **2016**, *120*, 9287–9296, PMID: 27571288.

(26) Vazdar, M.; Wernersson, E.; Khabiri, M.; Cwiklik, L.; Jurkiewicz, P.; Hof, M.; Mann, E.; Kolusheva, S.; Jelinek, R.; Jungwirth, P. Aggregation of Oligoarginines at Phospholipid Membranes: Molecular Dynamics Simulations, Time-Dependent Fluorescence Shift, and Biomimetic Colorimetric Assays. *The Journal of Physical Chemistry B* **2013**, *117*, 11530–11540, PMID: 24020922.

(27) Allolio, C.; Magarkar, A.; Jurkiewicz, P.; Baxová, K.; Javanainen, M.; Mason, P. E.; Šachl, R.; Cebecauer, M.; Hof, M.; Horinek, D. et al. Arginine-rich cell-penetrating peptides induce membrane multilamellarity and subsequently enter via formation of a fusion pore. *Proceedings of the National Academy of Sciences* **2018**, *115*, 11923–11928.

(28) Brock, D. J.; Kustigian, L.; Jiang, M.; Graham, K.; Wang, T.-Y.; Erazo-Oliveras, A.; Najjar, K.; Zhang, J.; Rye, H.; Pellois, J.-P. Efficient cell delivery mediated by lipid-specific endosomal escape of supercharged branched peptides. *Traffic (Copenhagen, Denmark)* **2018**, *19*, 421—435.

(29) Brock, D. J.; Kondow-McConaghy, H.; Allen, J.; Brkljača, Z.; Kustigian, L.; Jiang, M.; Zhang, J.; Rye, H.; Vazdar, M.; Pellois, J.-P. Mechanism of Cell Penetration by Permeabilization of Late Endosomes: Interplay between a Multivalent TAT Peptide and Bis(monoacylglycero)phosphate. *Cell Chemical Biology* **2020**, *27*, 1296–1307.e5.

(30) Pujals, S.; Miyamae, H.; Afonin, S.; Murayama, T.; Hirose, H.; Nakase, I.; Taniuchi, K.; Umeda, M.; Sakamoto, K.; Ulrich, A. S. et al. Curvature Engineering: Positive Membrane Curvature Induced by Epsin N-Terminal Peptide Boosts Internalization of Octaarginine. *ACS Chemical Biology* **2013**, *8*, 1894–1899, PMID: 23834464.

(31) Kumara, B.; Wijesiri, N.; Rathnayake, P.; Ranatunga, R. A Re-evaluation of the Free Energy Profiles for Cell-Penetrating Peptides Across DOPC Membranes. *International Journal of Peptide Research and Therapeutics* **2021**, 1–13.

(32) Gao, X.; Hong, S.; Liu, Z.; Yue, T.; Dobnikar, J.; Zhang, X. Membrane potential drives direct translocation of cell-penetrating peptides. *Nanoscale* **2019**, *11*, 1949–1958.

(33) Wang, B.; Zhang, J.; Zhang, Y.; Mao, Z.; Lu, N.; Liu, Q. H. The penetration of a charged peptide across a membrane under an external electric field: a coarse-grained molecular dynamics simulation. *RSC advances* **2018**, *8*, 41517–41525.

(34) Sakamoto, K.; Morishita, T.; Aburai, K.; Sakai, K.; Abe, M.; Nakase, I.; Futaki, S.; Sakai, H. Key Process and Factors Controlling the Direct Translocation of Cell-Penetrating Peptide through Bio-Membrane. *International Journal of Molecular Sciences* **2020**, *21*.

(35) Sakamoto, K.; Morishita, T.; Aburai, K.; Ito, D.; Imura, T.; Sakai, K.; Abe, M.; Nakase, I.; Futaki, S.; Sakai, H. Direct entry of cell-penetrating peptide can be controlled by maneuvering the membrane curvature. *International Journal of Molecular Sciences* **2021**, *11*.

(36) Krüger, D.; Ebenhan, J.; Werner, S.; Bacia, K. Measuring Protein Binding to Lipid Vesicles by Fluorescence Cross-Correlation Spectroscopy. *Biophysical Journal* **2017**, *113*, 1311–1320.

(37) Leontyev, I. V.; Stuchebrukhov, A. A. Electronic continuum model for molecular dynamics simulations of biological molecules. *Journal of chemical theory and computation* **2010**, *6*, 1498–1508.

(38) Kirby, B. J.; Jungwirth, P. Charge scaling manifesto: A way of reconciling the inherently macroscopic and microscopic natures of molecular simulations. *The journal of physical chemistry letters* **2019**, *10*, 7531–7536.

(39) Melcr, J.; Martinez-Seara, H.; Nencini, R.; Kolafa, J.; Jungwirth, P.; Ollila, O. H. S. Accurate Binding of Sodium and Calcium to a POPC Bilayer by Effective Inclusion of

Electronic Polarization. *The Journal of Physical Chemistry B* **2018**, *122*, 4546–4557, PMID: 29608850.

(40) Melcr, J.; Ferreira, T. M.; Jungwirth, P.; Ollila, O. S. Improved cation binding to lipid bilayers with negatively charged POPS by effective inclusion of electronic polarization. *Journal of chemical theory and computation* **2019**, *16*, 738–748.

(41) Duboué-Dijon, E.; Javanainen, M.; Delcroix, P.; Jungwirth, P.; Martinez-Seara, H. A practical guide to biologically relevant molecular simulations with charge scaling for electronic polarization. *The Journal of Chemical Physics* **2020**, *153*, 050901.

(42) Nencini, R.; Tempra, C.; Biriukov, D.; Polák, J.; Ondo, D.; Heyda, J.; Ollila, S. O.; Javanainen, M.; Martinez-Seara, H. Prosecco: polarization reintroduced by optimal scaling of electronic continuum correction origin in MD simulations. *Biophysical Journal* **2022**, *121*, 157a.

(43) Marquardt, D.; Heberle, F. A.; Miti, T.; Eicher, B.; London, E.; Katsaras, J.; Pabst, G. ^{1}H NMR shows slow phospholipid flip-flop in gel and fluid bilayers. *Langmuir* **2017**, *33*, 3731–3741.

(44) Lorent, J.; Levental, K.; Ganesan, L.; Rivera-Longsworth, G.; Sezgin, E.; Doktorova, M.; Lyman, E.; Levental, I. Plasma membranes are asymmetric in lipid unsaturation, packing and protein shape. *Nature chemical biology* **2020**, *16*, 644–652.

(45) Ramírez, P. G.; Del Pópolo, M. G.; Vila, J. A.; Szleifer, I.; Longo, G. S. Adsorption and insertion of polyarginine peptides into membrane pores: The trade-off between electrostatics, acid-base chemistry and pore formation energy. *Journal of Colloid and Interface Science* **2019**, *552*, 701–711.

(46) Klauda, J.; Venable, R.; Freites, J.; O'Connor, J.; Tobias, D.; Mondragon-Ramirez, C.; Vorobyov, I.; MacKerell, A. J.; Pastor, R. Update of the CHARMM all-atom additive

force field for lipids: validation on six lipid types. *The journal of physical chemistry B* **2010**, *114*, 7830–43.

(47) Kohagen, M.; Mason, P. E.; Jungwirth, P. Accurate Description of Calcium Solvation in Concentrated Aqueous Solutions. *The Journal of Physical Chemistry B* **2014**, *118*, 7902–7909, PMID: 24802184.

(48) Kohagen, M.; Mason, P. E.; Jungwirth, P. Accounting for Electronic Polarization Effects in Aqueous Sodium Chloride via Molecular Dynamics Aided by Neutron Scattering. *The Journal of Physical Chemistry B* **2016**, *120*, 1454–1460, PMID: 26172524.

(49) Martinek, T.; Duboué-Dijon, E.; Timr, Š.; Mason, P. E.; Baxová, K.; Fischer, H. E.; Schmidt, B.; Pluhařová, E.; Jungwirth, P. Calcium ions in aqueous solutions: Accurate force field description aided by ab initio molecular dynamics and neutron scattering. *The Journal of chemical physics* **2018**, *148*, 222813.

(50) Leontyev, I.; Stuchebrukhov, A. Accounting for electronic polarization in non-polarizable force fields. *Phys. Chem. Chem. Phys.* **2011**, *13*, 2613–2626.

(51) Catte, A.; Girych, M.; Javanainen, M.; Loison, C.; Melcr, J.; Miettinen, M. S.; Monticelli, L.; Määttä, J.; Oganesyan, V. S.; Ollila, O. H. S. et al. Molecular electrometer and binding of cations to phospholipid bilayers. *Phys. Chem. Chem. Phys.* **2016**, *18*, 32560–32569.

(52) Jorgensen, W. L.; Chandrasekhar, J.; Madura, J. D.; Impey, R. W.; Klein, M. L. Comparison of simple potential functions for simulating liquid water. *The Journal of chemical physics* **1983**, *79*, 926–935.

(53) Durell, S. R.; Brooks, B. R.; Ben-Naim, A. Solvent-induced forces between two hydrophilic groups. *The Journal of Physical Chemistry* **1994**, *98*, 2198–2202.

(54) Páll, S.; Hess, B. A flexible algorithm for calculating pair interactions on SIMD architectures. *Computer Physics Communications* **2013**, *184*, 2641–2650.

(55) Essmann, U.; Perera, L.; Berkowitz, M. L.; Darden, T.; Lee, H.; Pedersen, L. G. A smooth particle mesh Ewald method. *The Journal of Chemical Physics* **1995**, *103*, 8577–8593.

(56) Darden, T.; York, D.; Pedersen, L. Particle mesh Ewald: An N·log (N) method for Ewald sums in large systems. *The Journal of chemical physics* **1993**, *98*, 10089–10092.

(57) Berendsen, H. J. C.; Postma, J. P. M.; van Gunsteren, W. F.; DiNola, A.; Haak, J. R. Molecular dynamics with coupling to an external bath. *The Journal of Chemical Physics* **1984**, *81*, 3684–3690.

(58) Parrinello, M.; Rahman, A. Polymorphic transitions in single crystals: A new molecular dynamics method. *Journal of Applied Physics* **1981**, *52*, 7182–7190.

(59) Shuichi, N. A molecular dynamics method for simulations in the canonical ensemble. *Molecular Physics* **1984**, *52*, 255–268.

(60) Hoover, W. G. Canonical dynamics: Equilibrium phase-space distributions. *Phys. Rev. A* **1985**, *31*, 1695–1697.

(61) Hess, B.; Bekker, H.; Berendsen, H. J. C.; Fraaije, J. G. E. M. LINCS: A linear constraint solver for molecular simulations. *Journal of Computational Chemistry* **1997**, *18*, 1463–1472.

(62) Hess, B. P-LINCS: A Parallel Linear Constraint Solver for Molecular Simulation. *Journal of Chemical Theory and Computation* **2008**, *4*, 116–122, PMID: 26619985.

(63) Miyamoto, S.; Kollman, P. A. Settle: An analytical version of the SHAKE and RATTLE algorithm for rigid water models. *Journal of Computational Chemistry* **1992**, *13*, 952–962.

(64) Abraham, M. J.; Murtola, T.; Schulz, R.; Páll, S.; Smith, J. C.; Hess, B.; Lindahl, E. GROMACS: High performance molecular simulations through multi-level parallelism from laptops to supercomputers. *SoftwareX* **2015**, *1-2*, 19–25.

(65) Páll, S.; Zhmurov, A.; Bauer, P.; Abraham, M.; Lundborg, M.; Gray, A.; Hess, B.; Lindahl, E. Heterogeneous parallelization and acceleration of molecular dynamics simulations in GROMACS. *The Journal of Chemical Physics* **2020**, *153*, 134110.

(66) Michaud-Agrawal, N.; Denning, E. J.; Woolf, T. B.; Beckstein, O. MDAnalysis: A toolkit for the analysis of molecular dynamics simulations. *Journal of Computational Chemistry* **2011**, *32*, 2319–2327.

(67) Barducci, A.; Bussi, G.; Parrinello, M. Well-Tempered Metadynamics: A Smoothly Converging and Tunable Free-Energy Method. *Physical Review Letters* **2008**, *100*, 020603.

(68) Tribello, G. A.; Bonomi, M.; Branduardi, D.; Camilloni, C.; Bussi, G. PLUMED 2: New feathers for an old bird. *Computer Physics Communications* **2014**, *185*, 604–613.

(69) Sun, W.-C.; Gee, K. R.; Klaubert, D. H.; Haugland, R. P. Synthesis of Fluorinated Fluoresceins. *The Journal of Organic Chemistry* **1997**, *62*, 6469–6475.

(70) Gutfreund, H. Binding and Linkage: Functional chemistry of biological macromolecules. *FEBS Letters* **1991**, *293*, 224–224.

(71) Takechi, Y.; Tanaka, H.; Kitayama, H.; Yoshii, H.; Tanaka, M.; Saito, H. Comparative study on the interaction of cell-penetrating polycationic polymers with lipid membranes. *Chemistry and Physics of Lipids* **2012**, *165*, 51–58.

(72) Åmand, H. L.; Fant, K.; Nordén, B.; Esbjörner, E. K. Stimulated endocytosis in penetratin uptake: Effect of arginine and lysine. *Biochemical and Biophysical Research Communications* **2008**, *371*, 621–625.

(73) Hughes, L. D.; Rawle, R. J.; Boxer, S. G. Choose Your Label Wisely: Water-Soluble Fluorophores Often Interact with Lipid Bilayers. *PLOS ONE* **2014**, *9*, 1–8.

(74) Irvin, R. T.; MacAlister, T. J.; Costerton, J. W. Tris(hydroxymethyl)aminomethane buffer modification of Escherichia coli outer membrane permeability. *Journal of Bacteriology* **1981**, *145*, 1397–1403.

(75) Wolde-Kidan, A.; Netz, R. R. Interplay of Interfacial Viscosity, Specific-Ion, and Impurity Adsorption Determines Zeta Potentials of Phospholipid Membranes. *Langmuir* **2021**, *37*, 8463–8473, PMID: 34236206.

(76) Pielak, G. J. Buffers, Especially the Good Kind. *Biochemistry* **2021**, *60*, 3436–3440, PMID: 33939915.

(77) He, X.; Lin, M.; Guo, J.; Qu, Z.; Xu, F. Experimental and simulation studies of polyarginines across the membrane of giant unilamellar vesicles. *RSC Adv.* **2016**, *6*, 30454–30459.

(78) Tesei, G.; Vazdar, M.; Jensen, M. R.; Cragnell, C.; Mason, P. E.; Heyda, J.; Skepö, M.; Jungwirth, P.; Lund, M. Self-association of a highly charged arginine-rich cell-penetrating peptide. *Proceedings of the National Academy of Sciences* **2017**, *114*, 11428–11433.

(79) Khomich, D. A.; Nesterenko, A. M.; Kostritskii, A. Y.; Kondinskaia, D. A.; Ermakov, Y. A.; Gurtovenko, A. A. Independent adsorption of monovalent cations and cationic polymers at PE/PG lipid membranes. *Journal of Physics: Conference Series* **2017**, *794*, 012010.

(80) Javanainen, M.; Melcrová, A.; Magarkar, A.; Jurkiewicz, P.; Hof, M.; Jungwirth, P.; Martinez-Seara, H. Two cations, two mechanisms: interactions of sodium and calcium with zwitterionic lipid membranes. *Chemical Communications* **2017**, *53*, 5380–5383.